Earthquakes and Structures, *Vol. 30, No. 5 (2026) 665-685*
https://doi.org/10.12989/eas.2026.30.5.665

Numerical analysis of the seismic performance of H-shaped steel joints with initial defects

Yuan Zuo*[1], Weibin Li[2]

[1]*School of Economics and Management, Nanjing Vocational University of Industry Technology, 210023, Nanjing, China*
[2]*School of Civil Engineering, Southeast University, 210096, Nanjing, China*

(Received February 28, 2026, Revised March 26, 2026, Accepted April 6, 2026)

Abstract. The welding quality of beam-column joints of steel structures is one of the most important factors affecting seismic behavior of steel structures. In order to investigate the influence of initial defects on the seismic performance of H-shaped beam-column joints, the extended finite element method was used. A crack was set at the lower flange weld of H-shaped beam-column joints, and the influence of defect position and defect depth on the seismic performance was examined. The loading methods with different amplitudes were adopted. The research findings indicate that the initial defect exerts a significant influence on the seismic performance of the joint. The bearing capacity and energy dissipation capacity of the joints were decreased, and the degree of reduction accelerates with the increase of defect depth. However, the loading amplitude has a relatively minor effect on the seismic performance of the joint, with a maximum difference of 6.97% and an average difference of 0.31% in ultimate bending moment. Similarly, the influence of the initial defect location is limited, with a maximum difference of 11.9% and an average difference of 3.6%.

Keywords: extended finite element method; seismic properties; steel beam-column joint

1. Introduction

There are likely to be various defects, to a greater or lesser extent, in the weld of the steel structure beam-column joint. Moreover, the weld quality of field welding sometimes fails to meet the welding quality requirements specified in the relevant specification. Under the action of external loads, these defects will further expand and eventually lead to the fracture of the joint weld area [1, 2].

At present, numerous studies have been carried out by domestic and foreign scholars on joints with initial defects. Wang et al. [3, 4] established a finite element model and investigated the influence of defect size and location on the fracture toughness requirement of joint materials from the perspective of fracture mechanics. For high-strength steel connections, fracture behavior has been evaluated using elastic stress intensity factors and inelastic J-integral, leading to improved weld details [5]. Li et al. [6] conducted experimental research on the fracture performance of local weld specimens, revealing the influence of weld details on crack propagation behavior.

*Corresponding author, Ph.D., E-mail: zuoyuan5@126.com

http://www.techno-press.org/eas/5

ISSN: 2092-7614 (Print), 2092-7622 (Online)

Micromechanics damage models have been employed to simulate crack initiation and propagation in welded joints under monotonic and cyclic loading conditions, enabling analysis of void growth and fatigue life prediction [7]. Systematic parametric finite element analyses have been conducted to investigate the effects of weld access hole geometry, beam web welding, and continuity plates on the inelastic cyclic performance of welded beam-to-column connections [8]. Azuma et al. [9] performed repeated loading tests and finite element analysis on 4 full-scale beam-column joints with initial defects, and believe that the defect propagation and failure behavior of the beam-column joints vary significantly depending on different defect types. Liu et al. established finite element models of diaphragm through-type beam-column joints with and without defects with reference to the experiment on the external weld defect of the arc crater, and applied low-cycle reciprocating cyclic loads to predict the ductile fracture of the joint. Probabilistic seismic risk assessment methodologies, such as fragility analysis, have been applied to evaluate the performance of building frames under different ground motion conditions [11]. In addition, integrated experimental-numerical approaches combining shake table tests with fiber-based finite element modeling have been demonstrated to effectively capture the seismic behavior of structural systems [12], offering valuable methodological references for the assessment of welded joints with initial defects.

At present, there exists a relatively limited number of experiments and finite element studies focusing on the fracture failure mode and mechanical properties of steel structure beam-column joints resulting from the initial defect in the weld area. In this paper, the influence of the initial defect on the seismic performance of the H-shaped steel joint is further investigated from the perspectives of the initial defect position, the initial defect size, and the loading mode.

2. Establishment of the finite element model

2.1 Initial defect design

The extended finite element method is employed to analyze the fracture performance of the beam-column joint. In this study, the XFEM analysis is implemented using ABAQUS (version 2022), which provides an XFEM module that enables effective simulation of defect initiation and propagation in the weld region. The validation of the finite element model is based on experimental data from two representative specimens: one without initial defects, and one with an initial defect of 1.0 mm depth located at the middle of the lower flange weld [13]. Both specimens were tested under the same variable amplitude cyclic loading protocol. The close agreement between the numerical predictions and experimental results for both specimens confirms the reliability of the XFEM approach for simulating the mechanical behavior of welded beam-column joints with initial defects. The stiffness ratio of the beam-column I_b/I_c is 0.42, the beam section has dimensions of 400 mm×150 mm×8 mm×12 mm, while the column section has dimensions of 450 mm×250 mm×12 mm×16 mm, and the hexahedral element (Hex) is selected for the simulation. Without considering the influence of bolt welding factors, the joint is simplified to full welding. The A end of the column is fixed, and the B end of the column restricted all but the vertical displacement, thereby having five degrees of freedom restricted. The loading mode adopted involves the application of in-plane vertical displacement at the beam end. The element size of the finite element model is refined in the region near the joint, and the minimum element size near the weld of the lower flange of the beam is selected as 1.0 mm. CRACK is used to simulate the initial

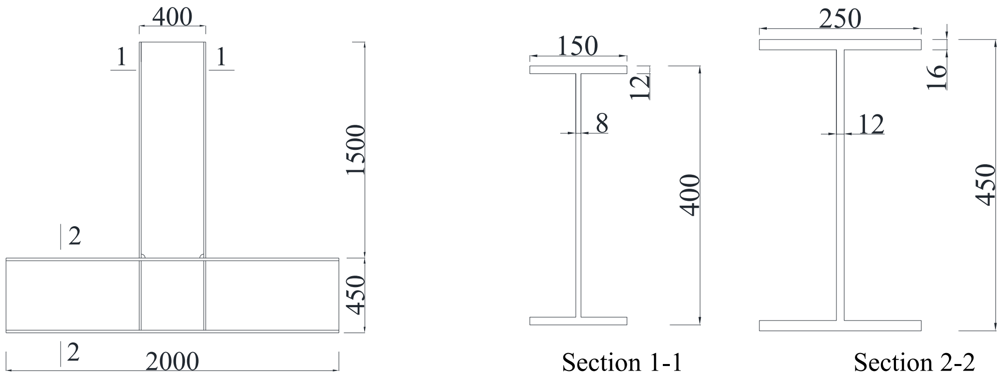

(a) The dimensions of the joint specimen (b) Cross-sectional dimensions of beam and column

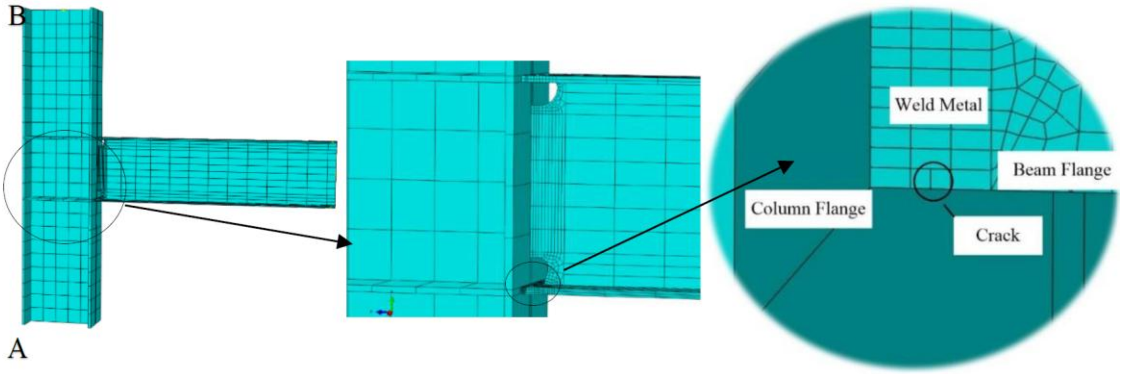

(c) Finite element model of the joint (d) Mesh refinement at the connection (e) Detailed view of initial defect

Figure 1. Finite element model of H-shaped beam-column joint (All dimensions in mm)

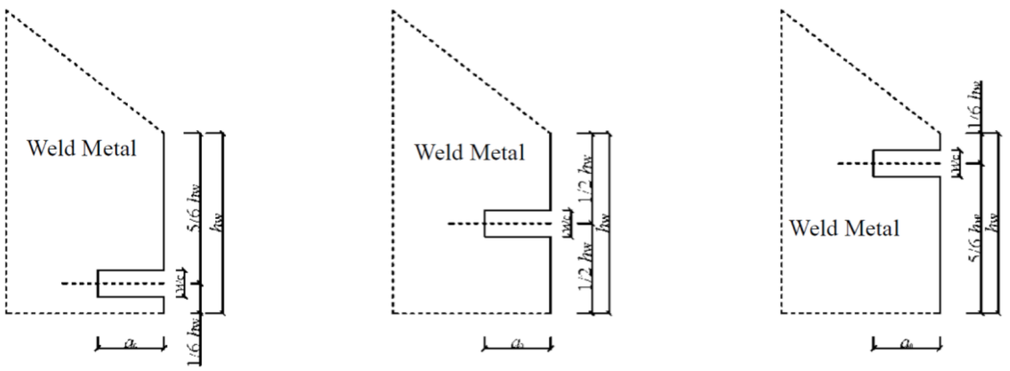

(a) Left side (b) Middle (c) Right side

Figure 2. Schematic diagram of initial defect positions in the weld area of the lower flange (Notes: a_0=depth of the initial defect; w_c=width of the initial defect; h_w=height of the weld external side)

defect of the joint, and the finite element model is depicted in Fig. 1. The CRACK module in ABAQUS was employed to model the initial defect of the joint, as illustrated in Fig. 2. Crack

Table 1. Material properties of Q345 steel and E5015 electrodes [15]

Material (MPa)	Q345 (16 mm)	Q345 (12 mm)	Q345 (8 mm)	E5015
Yield strength	392.7	360.1	353.8	391.4
Ultimate strength	548.2	479.6	428.3	615.8

propagation was analyzed using the extended finite element method (XFEM) based on linear elastic fracture mechanics, which enables crack growth along an arbitrary path. The maximum principal stress criterion was adopted for crack initiation and propagation. Once the calculated maximum principal stress satisfied the criterion, the crack began to propagate, with the crack surfaces displacing in the direction of the external load, resulting in crack growth along the perpendicular direction.

In order to investigate the influence of the defect position on the seismic performance of the rigid joint [1, 13], the initial defect position is shown in Fig. 2.

2.2 Material properties

The joint adopts Q345 steel and E50 electrodes. The elastic modulus is 2.06×10^5 MPa and the elongation rate is 23%. In accordance with the current code, a bilinear constitutive model (defined by the yield strength and ultimate strength) is adopted in the finite element simulation [14]. The material properties are shown in Table 1.

2.3 Loading system

The initial defect depth is set within the range of a_0=0.0 mm to 8.0 mm, and the performance parameters of the characteristic points (yield point, limit point) of the joint with the initial defect under the action of external loads are investigated. The estimated yield displacement of the joint is Δy=15 mm. The loading protocols adopted in this study (B, C, D, E, F, G, H, as shown in Fig. 3) are designed with reference to the standard cyclic loading procedures recommended in the Specification for Seismic Test of Buildings [16]. When the loading systems of B, C, and D are selected, the increment of each stage is controlled according to 0.25 times the estimated yield displacement [17], and each stage is cycled twice to minimize the experimental error. The loading systems of B, C, and D represent variable amplitude loading, while E, F, G, and H represent constant amplitude loading [15]. The bending moment and rotation value are considered positive when the lower flange of the beam is in tension and negative when it is in compression. The loading is terminated and the joint is deemed damaged when the tension on one side of the beam breaks. This study focuses on the influence of the location, depth, and loading protocol of initial defects on the seismic performance of the joint, with particular emphasis on damage evolution and failure modes under cyclic lateral loading at the beam end. Therefore, the effect of axial load on the column is not considered in the finite element model.

3. Finite element phenomena and analysis.

The specimen numbering method described in the text is as follows: the first digit (where 1, 2,

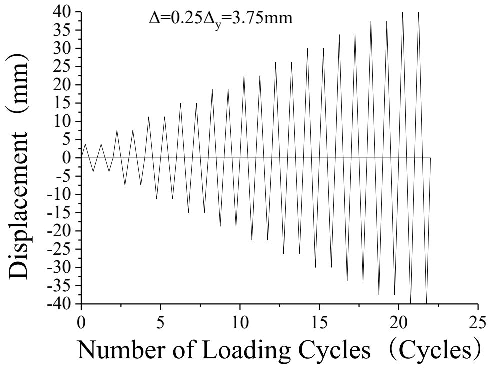

(a)Variable amplitude loading system B

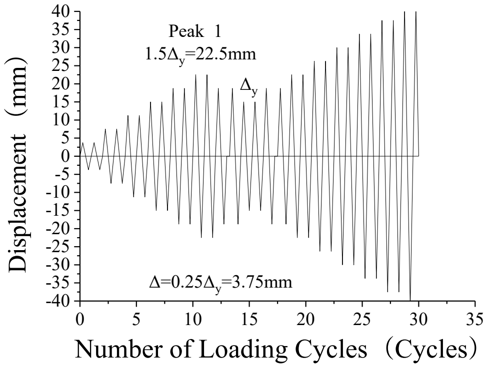

(b) Variable amplitude loading system C

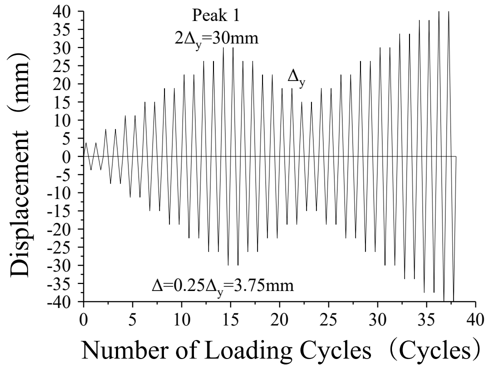

(c) Variable amplitude loading system D

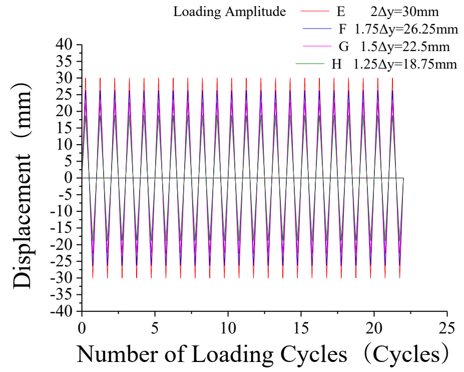

(d) Constant amplitude loading systems (E, F, G, H) with varying displacement amplitudes

Figure 3. Loading protocols

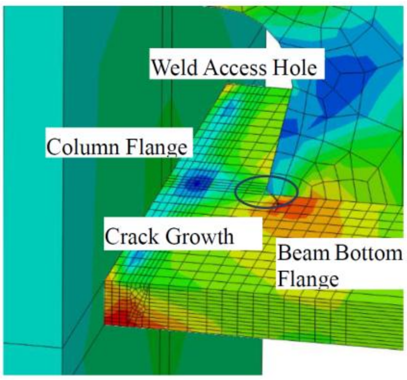

(a) Crack initiation at the weld access hole

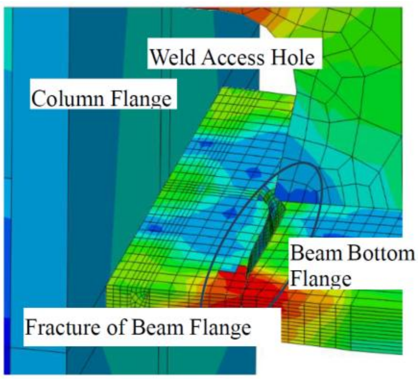

(b) Flange fracture after crack propagation

Figure 4. Crack initiation and propagation in specimen without initial defect (B-0)

and 3 on the left, middle, and right respectively represent 1, 2, and 3) indicates the position of the initial defect within the weld area of the lower flange of the beam. The letter (B, C, D, E, F, G, H) represents the loading method, and the second digit (ranging from 0.0 mm to 8.0 mm) indicates the depth of the initial defect in the steel joint.

Table 2. Ultimate bending moment M_u (kN·m) and ultimate rotation angle ϕ_u (rad) of specimens without initial defect (a_0=0.0 mm) under different loading systems (B-H)

No.	Direction of force application	Ultimate bending moment M_u (kN·m)	Ultimate rotation angle ϕ_u (rad)	No.	Direction of force application	Ultimate bending moment M_u (kN·m)	Ultimate rotation angle ϕ_u (rad)
B-0	positive	377.7870	0.0199	F-0	positive	377.6580	0.0171
	negative	-395.0730	-0.0198		negative	-388.9000	-0.0175
C-0	positive	377.9820	0.0198	G-0	positive	374.5380	0.0149
	negative	-390.4000	-0.0195		negative	-379.3000	-0.0150
D-0	positive	377.7870	0.0199	H-0	positive	320.6000	0.0123
	negative	-395.0730	-0.0198		negative	-325.7000	-0.0125
E-0	positive	380.1300	0.0200				
	negative	-395.9000	-0.0199				

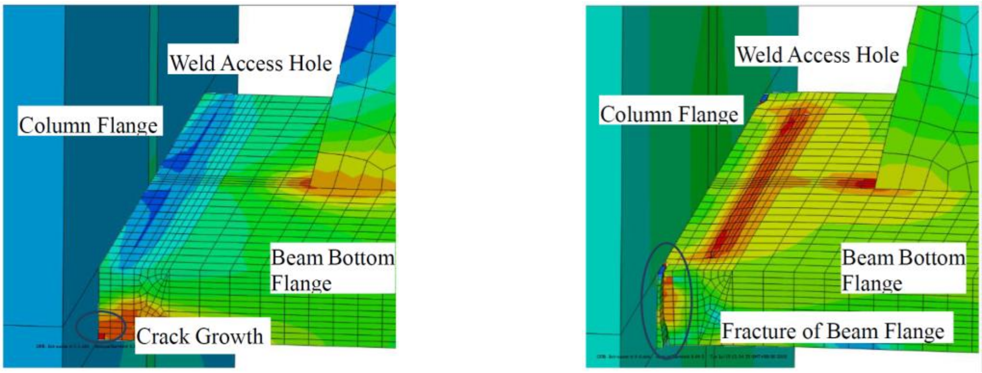

(a) Crack tip fracture (b)Complete fracture of the lower flange

Figure 5. Crack propagation in specimen with initial defect on the left side of the lower flange weld (1-B-1)

3.1 The weld area of the lower flange of the beam without an initial defect

Taking the component B-0 as an example, when the specimen is loaded to the 10th cycle and the beam end displacement is 11.911 mm and the force is 130.844 kN, cracks first appear at the junction of the welded hole in the lower flange of the beam and the lower flange of the beam, as depicted in Fig. 4(a). Under the reciprocating load of the beam-column joint, owing to the large local stiffness and stress concentration at the junction of the welded hole in the lower flange of the beam and the lower flange of the beam, the crack initiates first at the junction and then expands towards both sides of the flange, as shown in Fig. 4(b). Eventually, the beam flange fractures. The bearing capacity and deformability of the specimen are shown in Table 2.

3.2 The initial defect on the left side of the weld area of the lower flange of the beam

Taking the component 1-B-1 as an example, when the specimen is loaded to the 8th cycle with the beam end displacement being 17.406 mm and the force at 194.064 kN, the crack tip of the

Table 3. Ultimate bending moment M_u (kN·m) of joints with initial defects on the left side of the lower flange weld under different loading systems (B-H)

Loading modes	Force direction	a_0=1.0 mm	a_0=2.0 mm	a_0=3.0 mm	a_0=4.0 mm	a_0=5.0 mm	a_0=6.0 mm	a_0=7.0 mm	a_0=8.0 mm
B	Positive	339.5800	315.6600	276.4620	253.8000	240.7770	233.6440	192.4700	174.3000
	Negative	-339.4000	-334.8000	-258.2000	-251.0000	-259.5000	-192.3000	-195.7000	-197.8000
C	Positive	336.5490	315.6600	276.4620	253.8000	240.7770	233.6440	192.4700	174.3000
	Negative	-343.3000	-334.8000	-258.2000	-251.0000	-259.5000	-192.3000	-195.7000	-197.8000
D	Positive	339.5800	315.6600	276.4620	253.8000	240.7770	233.6440	192.4700	174.3000
	Negative	-339.4000	-334.8000	-258.2000	-251.0000	-259.5000	-192.3000	-195.7000	-197.8000
E	Positive	360.9000	321.2580	304.7910	271.1200	254.2110	232.4100	232.3500	209.6700
	Negative	-360.4710	0.0000	0.0000	0.0000	0.0000	0.0000	0.0000	0.0000
F	Positive	351.1900	317.4120	301.4310	285.3400	266.8230	250.2800	226.5000	205.9300
	Negative	-350.2000	0.0000	0.0000	0.0000	0.0000	0.0000	0.0000	0.0000
G	Positive	350.1000	310.4800	298.0000	280.4500	262.8400	244.6440	222.2040	200.5320
	Negative	-354.4740	0.0000	0.0000	0.0000	0.0000	0.0000	0.0000	0.0000
H	Positive	311.5696	302.8590	293.7330	276.9200	257.2080	237.6200	214.9900	192.9900
	Negative	-313.4490	-308.7000	-305.6000	-307.1280	0.0000	0.0000	0.0000	0.0000

Table 4. Ultimate rotation angle ϕ_u (rad) of joints with initial defects on the left side of the lower flange weld under different loading systems (B-H)

Loading modes	Force direction	a_0=1.0 mm	a_0=2.0 mm	a_0=3.0 mm	a_0=4.0 mm	a_0=5.0 mm	a_0=6.0 mm	a_0=7.0 mm	a_0=8.0 mm
B	Positive	0.0159	0.0150	0.0115	0.0107	0.0098	0.0097	0.0081	0.0075
	Negative	-0.0149	-0.0147	-0.0098	-0.0095	-0.0098	-0.0073	-0.0074	-0.0074
C	Positive	0.0148	0.0150	0.0115	0.0107	0.0098	0.0097	0.0081	0.0075
	Negative	-0.0151	-0.0147	-0.0098	-0.0095	-0.0098	-0.0073	-0.0074	-0.0074
D	Positive	0.0159	0.0150	0.0115	0.0107	0.0098	0.0097	0.0081	0.0075
	Negative	-0.0149	-0.0147	-0.0098	-0.0095	-0.0098	-0.0073	-0.0074	-0.0074
E	Positive	0.0198	0.0155	0.0139	0.0118	0.0120	0.0108	0.0109	0.0099
	Negative	-0.0199	0.0000	0.0000	0.0000	0.0000	0.0000	0.0000	0.0000
F	Positive	0.0161	0.0144	0.0133	0.0128	0.0116	0.0120	0.0108	0.0099
	Negative	-0.0154	0.0000	0.0000	0.0000	0.0000	0.0000	0.0000	0.0000
G	Positive	0.0150	0.0133	0.0130	0.0122	0.0113	0.0116	0.0106	0.0095
	Negative	-0.0149	0.0000	0.0000	0.0000	0.0000	0.0000	0.0000	0.0000
H	Positive	0.0125	0.0124	0.0125	0.0119	0.0111	0.0107	0.0103	0.0090
	Negative	-0.0122	-0.0124	-0.0121	-0.0123	0.0000	0.0000	0.0000	0.0000

initial defect on the beam flange breaks, as shown in Fig. 5(a). In comparison to the situation without defects, due to the reduction in the stressed area of the lower flange of the beam, cracks began to occur two cycles earlier in the node. When the defect is located on the left side of the

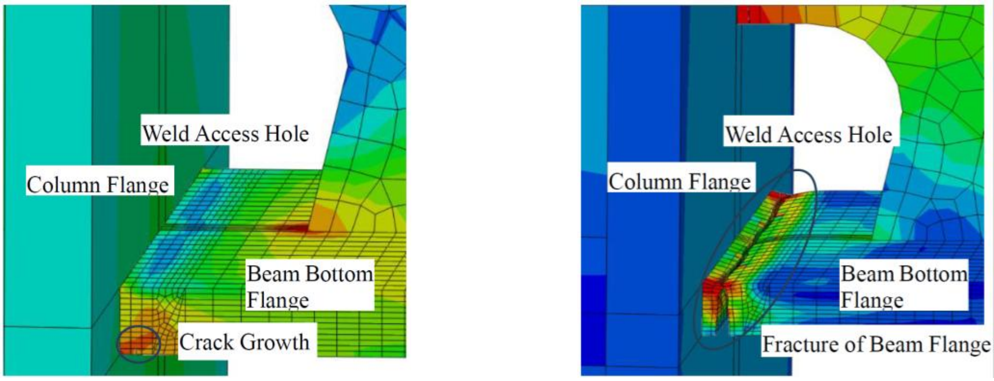

(a) Crack tip fracture (b) Complete fracture of the lower flange

Figure 6. Crack propagation in specimen with initial defect at the middle of the lower flange weld (2-B-1)

Table 5. Ultimate bending moment M_u (kN·m) of joints with initial defects at the middle of the lower flange weld under different loading systems (B-H)

Loading modes	Force direction	a_0=1.0 mm	a_0=2.0 mm	a_0=3.0 mm	a_0=4.0 mm	a_0=5.0 mm	a_0=6.0 mm	a_0=7.0 mm	a_0=8.0 mm
B	Positive	339.5250	303.7140	278.6970	247.8100	239.8440	225.4095	190.0900	167.7700
	Negative	-347.6000	-310.1000	-308.9100	-253.9000	-263.1180	-257.7000	-265.4000	-195.8370
C	Positive	338.8800	303.7140	278.3900	247.8100	239.8440	222.4100	190.0900	169.7700
	Negative	-346.5000	-310.1000	-308.9100	-253.9000	-263.1180	-257.7000	-193.6920	-195.8370
D	Positive	339.5250	303.7140	278.6970	247.8100	239.8440	222.4100	190.0900	169.7700
	Negative	-347.6000	-310.1000	-308.9100	-253.9000	-263.1180	-257.7000	-193.6920	-195.8370
E	Positive	335.5900	328.3700	309.1900	289.4900	254.6200	254.6200	242.5890	214.9500
	Negative	-357.7050	-358.3650	0.0000	0.0000	0.0000	0.0000	0.0000	0.0000
F	Positive	330.1125	327.5500	305.2020	285.9030	264.7050	249.6000	236.7180	207.0100
	Negative	-345.5400	-348.2000	0.0000	0.0000	0.0000	0.0000	0.0000	0.0000
G	Positive	344.2710	321.0000	302.2590	280.9200	258.9240	244.4490	229.5900	205.0500
	Negative	-349.0980	-332.5110	-331.9000	0.0000	0.0000	0.0000	0.0000	0.0000
H	Positive	318.3990	303.4900	249.8220	276.6300	255.4410	239.6400	222.1200	198.3600
	Negative	-318.8250	-312.1000	-305.2000	-309.6930	0.0000	0.0000	0.0000	0.0000

weld area of the lower flange, the stress at the crack is relatively high. Compared with the situation when a_0 is at the middle and right positions, the crack starts to develop at the earliest time. With the application of cyclic loads, the crack gradually develops until the flange is disconnected, as shown in Fig. 5(b). Eventually, the beam flange fractures. The bearing capacity and deformability of the specimen are shown in Tables 3 and 4 respectively.

3.3 The initial defect in the middle of the weld area of the lower flange of the beam

Taking the component 2-B-1 as an example, when the specimen is loaded to the 9.5th cycle, and the beam end displacement is 9.362 mm and the force is 117.678 kN, the crack tip of the initial

Table 6. Ultimate rotation angle ϕ_u (rad) of joints with initial defects at the middle of the lower flange weld under different loading systems (B-H)

Loading modes	Force direction	a_0=1.0 mm	a_0=2.0 mm	a_0=3.0 mm	a_0=4.0 mm	a_0=5.0 mm	a_0=6.0 mm	a_0=7.0 mm	a_0=8.0 mm
B	Positive	0.0150	0.0125	0.0118	0.0108	0.0100	0.0099	0.0092	0.0075
	Negative	-0.0150	-0.0125	-0.0124	-0.0096	-0.0099	-0.0098	-0.0100	-0.0074
C	Positive	0.0149	0.0125	0.0116	0.0108	0.0100	0.0099	0.0092	0.0075
	Negative	-0.0149	-0.0125	-0.0124	-0.0096	-0.0099	-0.0098	-0.0073	-0.0074
D	Positive	0.0150	0.0125	0.0118	0.0108	0.0100	0.0099	0.0092	0.0075
	Negative	-0.0150	-0.0125	-0.0124	-0.0096	-0.0099	-0.0098	-0.0073	-0.0074
E	Positive	0.0192	0.0184	0.0143	0.0128	0.0128	0.0128	0.0116	0.0108
	Negative	-0.0192	-0.0199	0.0000	0.0000	0.0000	0.0000	0.0000	0.0000
F	Positive	0.0168	0.0175	0.0139	0.0126	0.0124	0.0124	0.0112	0.0104
	Negative	-0.0168	-0.0174	0.0000	0.0000	0.0000	0.0000	0.0000	0.0000
G	Positive	0.0149	0.0149	0.0135	0.0122	0.0128	0.0118	0.0109	0.0099
	Negative	-0.0148	-0.0150	-0.0149	0.0000	0.0000	0.0000	0.0000	0.0000
H	Positive	0.0125	0.0125	0.0124	0.0119	0.0111	0.0113	0.0103	0.0095
	Negative	-0.0124	-0.0125	-0.0121	-0.0125	0.0000	0.0000	0.0000	0.0000

defect on the beam flange breaks, as shown in Fig. 6(a). In comparison to the situation without defects, due to the reduction of the stressed area of the lower flange of the beam, cracks began to occur one cycle earlier in the node. The cracking time is delayed compared to the moment when the defect occurs on the left side, and the fracture time of the lower flange is also delayed. With the application of cyclic loads, the crack gradually develops until the lower flange is disconnected, as shown in Fig. 6(b). Eventually, the beam flange fractures. The bearing capacity and deformability of the specimen are shown in Tables 5 and 6 respectively.

3.4 The initial defect on the right side of the weld area of the lower flange of the beam

Taking the component 3-B-1 as an example, when the specimen is loaded to the 9.5th cycle, and the beam end displacement is 18.50 mm and the force is 220.154 kN, the crack tip of the initial defect of the beam flange breaks, as shown in Fig. 7(a). In comparison to the situation without defects, due to the reduction of the stressed area of the lower flange of the beam, cracks began to occur half a cycle earlier in the node. When the crack is at the far right, the crack starts at the latest time among all positions, and the fracture of the lower flange also occurs at the latest time. With the application of cyclic loads, the crack gradually develops until the lower flange is disconnected, as shown in Fig. 7(b). Eventually, the beam flange fractures. The bearing capacity and deformability of the specimen are shown in Tables 7 and 8 respectively.

4. The influence of loading system on the performance of joints

The three loading systems of B, C, and D simulate the action modes that may occur in actual

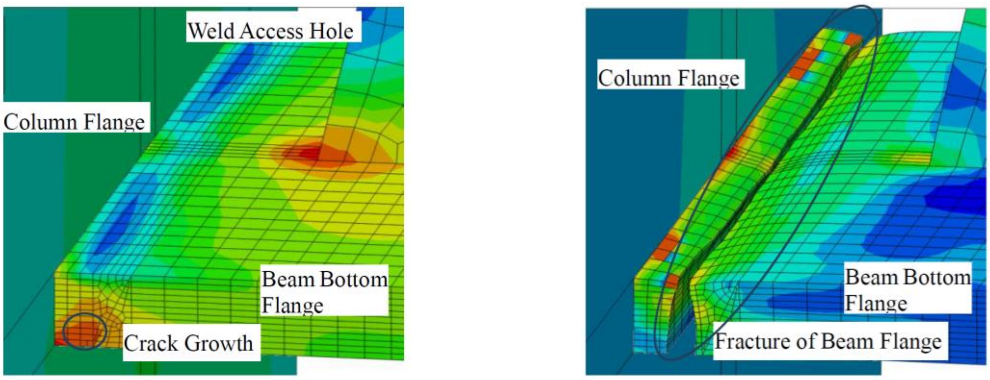

(a) Crack tip fracture (b) Complete fracture of the lower flange

Figure 7. Crack propagation in specimen with initial defect on the right side of the lower flange weld (3-B-1)

Table 7. Ultimate bending moment M_u (kN·m) of joints with initial defects on the right side of the lower flange weld under different loading systems (B-H)

Loading modes	Force direction	a_0=1.0 mm	a_0=2.0 mm	a_0=3.0 mm	a_0=4.0 mm	a_0=5.0 mm	a_0=6.0 mm	a_0=7.0 mm	a_0=8.0 mm
B	Positive	356.2500	303.0600	279.9400	279.9400	237.6500	225.4700	181.3170	170.2700
	Negative	-363.7000	-311.0070	-308.2000	-308.2000	-254.5290	-261.6180	-199.1760	-196.9000
C	Positive	346.2090	303.0600	279.9400	279.9400	237.2160	225.4700	180.3930	170.6200
	Negative	-349.5900	-311.0070	-308.2000	-308.2000	-263.3000	-261.6180	-198.6240	-197.9160
D	Positive	356.2500	302.3200	279.9400	279.9400	237.1890	222.6100	181.3170	170.6200
	Negative	-362.9000	-311.0070	-308.2000	-308.2000	-263.3000	-261.6180	-199.1820	-197.9160
E	Positive	336.4200	333.1300	307.8540	307.8540	288.5670	259.7200	243.0600	223.0710
	Negative	-358.0800	-357.1000	0.0000	0.0000	0.0000	0.0000	0.0000	0.0000
F	Positive	344.1400	329.5290	303.9960	303.9960	269.0340	256.6300	238.0050	223.0710
	Negative	-361.9320	-347.3000	-342.6000	-342.6000	0.0000	0.0000	0.0000	0.0000
G	Positive	332.3800	321.9800	300.9480	300.9480	265.7520	246.7170	232.1800	214.3110
	Negative	-342.6000	-332.5000	-332.4000	-332.4000	-329.4120	0.0000	0.0000	0.0000
H	Positive	306.8300	303.2200	294.3570	294.3570	260.5020	243.9780	226.2090	206.4510
	Negative	-310.2000	-310.2720	-309.9690	-309.9690	-306.0840	-310.3000	0.0000	0.0000

earthquakes. Subsequently, an analysis is conducted to explore the influence of the loading peak and sequence on the performance of the joint.

4.1 Variable amplitude cycle

As can be inferred from Tables 3 to 5, the ultimate bearing capacities of the specimens are remarkably close. Taking a_0=0.0 mm as an example, the ultimate bending moments of the components under the loading modes B, C, and D are 377.787 kN·m, 377.982 kN·m, and 377.787 kN·m, respectively. The skeleton curves for a0 values ranging from 0.0 mm to 8.0 mm are presented in Fig. 8. It can be observed from Fig. 8 that, for a given loading method, the skeleton

Table 8. Ultimate rotation angle ϕ_u (rad) of joints with initial defects on the right side of the lower flange weld under different loading systems (B-H)

Loading modes	Force direction	a_0=1.0 mm	a_0=2.0 mm	a_0=3.0 mm	a_0=4.0 mm	a_0=5.0 mm	a_0=6.0 mm	a_0=7.0 mm	a_0=8.0 mm
B	Positive	0.01750	0.0124	0.0120	0.0120	0.0100	0.0100	0.0074	0.0075
	Negative	-0.0172	-0.0125	-0.0123	-0.0123	-0.0096	-0.0100	-0.0075	-0.0074
C	Positive	0.0150	0.0124	0.0120	0.0120	0.0100	0.0100	0.0073	0.0075
	Negative	-0.0144	-0.0125	-0.0123	-0.0123	-0.0100	-0.0100	-0.0075	-0.0074
D	Positive	0.0175	0.0123	0.0120	0.0120	0.0100	0.0099	0.0074	0.0075
	Negative	-0.0171	-0.0125	-0.0123	-0.0123	-0.0100	-0.0100	-0.0075	-0.0074
E	Positive	0.0192	0.0199	0.0141	0.0141	0.0141	0.0126	0.0121	0.0116
	Negative	-0.0192	-0.0184	0.0000	0.0000	0.0000	0.0000	0.0000	0.0000
F	Positive	0.0155	0.0174	0.0138	0.0138	0.0133	0.0121	0.0116	0.0116
	Negative	-0.0174	-0.0173	-0.0171	-0.0171	0.0000	0.0000	0.0000	0.0000
G	Positive	0.0144	0.0150	0.0137	0.0137	0.0128	0.0120	0.0112	0.0109
	Negative	-0.0144	-0.0149	-0.0150	-0.0150	-0.0150	0.0000	0.0000	0.0000
H	Positive	0.0118	0.0124	0.0125	0.0125	0.0123	0.0117	0.0112	0.0100
	Negative	-0.0120	-0.0123	-0.0125	-0.0125	-0.0121	-0.0125	0.0000	0.0000

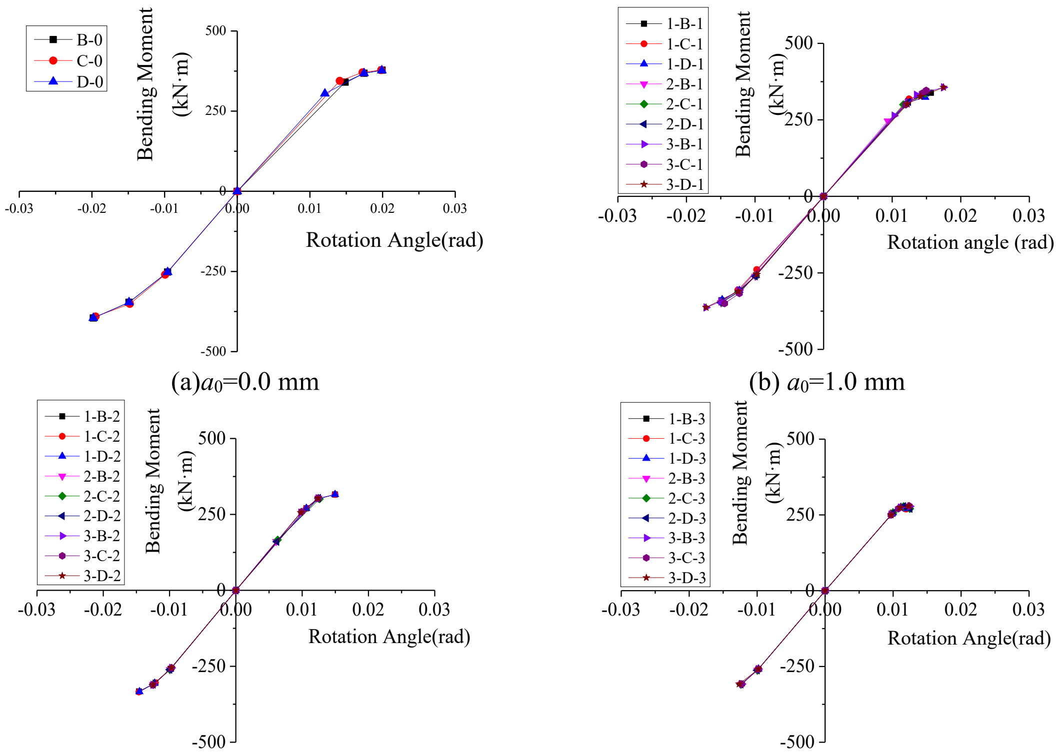

(a)a_0=0.0 mm (b) a_0=1.0 mm

(c) a_0=2.0 mm (d) a_0=3.0 mm

Figure 8. Skeleton curves of beam-column joints with different initial defects depths (a_0=0.0-8.0 mm) under variable amplitude loading systems (B, C, D)

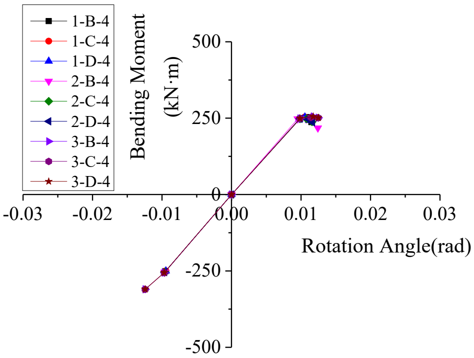

(e) a_0=4.0 mm

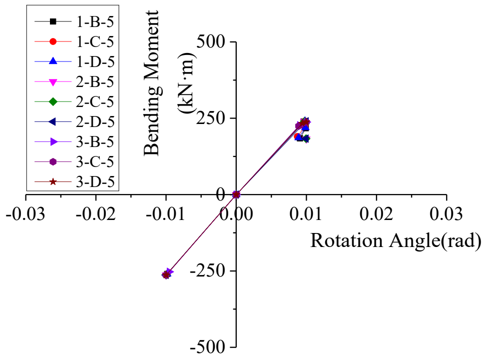

(f) a_0=5.0 mm

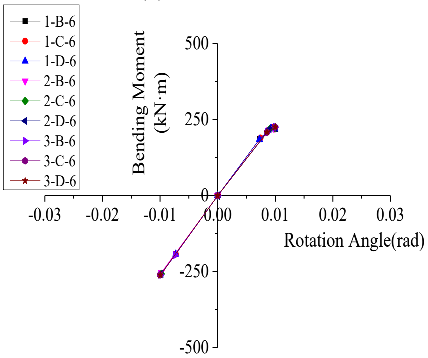

(g) a_0=6.0 mm

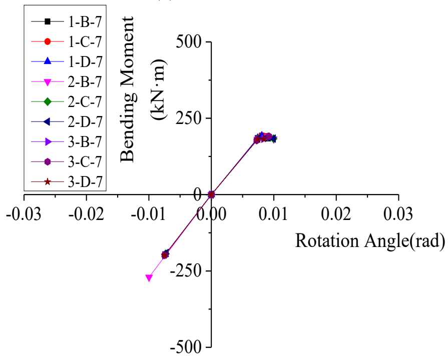

(h) a_0=7.0 mm

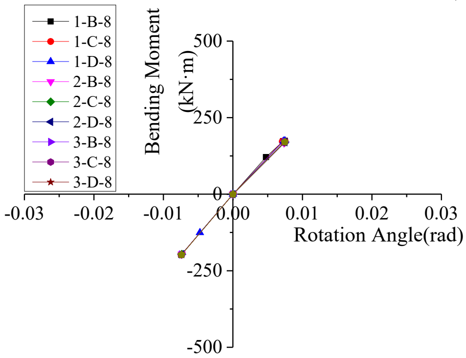

(i) a_0=8.0 mm

Figure 8. Continued

curves of components with different initial defect positions almost coincide.

It can be observed from Fig. 8:

1. Under the action of the variable amplitude loading systems B, C, and D, when the initial defect depth and location are identical, the ultimate bending moment and ultimate rotation angle values of the component do not differ much. By comparing the ultimate bending moment and rotation angle values of 1-B-1, 1-C-1, and 1-D-1 in Tables 3 and 4, it is found that when a_0=0.0 mm to 8.0 mm, the maximum difference is 6.97%, the minimum is 0%, and the average is 0.31%. Therefore, the loading amplitude is considered to have a negligible effect on the

ultimate bending moment and rotation angle of the joint, with the maximum difference being only 6.97%.

2. Under the same loading method, when the initial defect is located on the left, middle, or right side of the weld area of the lower flange of the beam, the ultimate bending moment and rotation angle values do not differ much. After the complete fracture of the lower flange of the beam, since the web of the joint remains under stress, the joint still possesses some bearing capacity, although the bearing capacity decreases rapidly. By comparing the ultimate bending moment and rotation angle values of 1-B-1 in Tables 3 and 4, 2-B-1 in Tables 5 and 6, and 3-B-1 in Tables 7 and 8, when a_0=0.0 mm to 8.0 mm, the minimum difference is 0.98%, the maximum is 11.9%, and the average difference is 3.6%, indicating that the influence of defect location is less critical compared with the effect of defect depth.

3. It can be observed from Fig. 8(b) to (i) that as the depth of the initial defect increases, under the same initial defect depth conditions, the influence of the displacement peak value of the loading system on the ultimate bending moment and ultimate rotation angle of the joint gradually diminishes. When a_0 1.0 mm, the skeleton curves of the joints exhibit slight differences. However, as the defect depth further increases, the skeleton curves of the joints tend to coincide. The reason for this phenomenon is that with increasing initial defect depth, the beam flange breaks rapidly after loading, the number of cycles of the component decreases, and the change in the bearing capacity of the component is not significant.

4. As can be inferred from Tables 3 to 8, as the depth of the defect increases, the ultimate bending moment and rotation angle of the joint gradually decrease, and the value of the decrease exhibits a nonlinear relationship with the defect depth.

5. As can be inferred from Fig. 8, the skeleton of the joint without the initial defect is relatively plump, and the energy dissipation capacity of the joint with the initial defect is better. This indicates that the initial defect will have a significant adverse effect on the bearing capacity and energy dissipation capacity of the joint.

4.2 Constant amplitude cycle

E, F, G, and H represent the constant amplitude cyclic loading systems with varying amplitudes, which are employed to verify the characteristics of the joint under the action of low-cycle fatigue loads. The ultimate bending moment and rotation angle values are presented in Tables 9 and 10, respectively. Based on the data presented in the tables:

1. Under the constant amplitude cyclic loading system, corresponding to different loading amplitudes, the ultimate bending moment value and the ultimate rotation angle value of the specimen decrease as the displacement loading amplitude decreases.

2. By comparing the components under the four constant amplitude loading modes of E, F, G, and H, it is found that the ultimate bending moment and ultimate rotation angle values are relatively small, which indicates that the smaller the loading amplitude of the component, the less sufficient the plasticity and strengthening will be, and its energy dissipation ability cannot be fully utilized. The failure mode of the joint is closer to low-cycle fatigue failure, and its ultimate bending moment is significantly reduced.

Through the finite element simulation analysis of the components under both the variable amplitude loading mode and the constant amplitude loading mode, it can be observed that under the same initial defect depth condition, neither the constant amplitude loading nor the variable amplitude loading has a significant influence on the performance of the joint.

Table 9. Ultimate bending moment M_u (kN·m) of joints with initial defects at different positions (left, middle, right) under constant amplitude loading systems (E, F, G, H)

Defect depths	Loading mode E (kN·m)			Loading mode F (kN·m)			Loading mode G (kN·m)			Loading mode H (kN·m)		
	Left	Middle	Right	Left	Middle	Right	Left	Middle	Right	Left	Middle	Right
a_0=0.0 mm		380.1300			377.6580			374.5380			323.0600	
a_0=1.0 mm	360.9000	335.5900	336.4200	351.1900	330.1120	344.1400	350.1000	344.2710	332.3800	311.5690	318.3990	306.8300
a_0=2.0 mm	321.2580	328.3700	333.1300	317.4120	327.5500	329.5290	310.4800	321.0000	321.9800	302.8590	303.4900	303.2200
a_0=3.0 mm	304.7910	309.1900	307.8540	301.4310	305.2020	303.9960	298.0000	302.2590	300.9480	293.7330	249.8220	294.3570
a_0=4.0 mm	271.1200	289.4900	288.4800	285.3400	285.9030	285.9500	280.4500	280.9200	283.0100	276.9200	276.6300	277.1940
a_0=5.0 mm	254.2110	254.6200	288.5670	266.8230	264.7050	269.0340	262.8400	258.9240	265.7520	257.2080	255.4410	260.5020
a_0=6.0 mm	232.4100	254.6200	259.7200	250.2800	249.6000	256.6300	244.6440	244.4490	246.7170	237.6200	239.6400	243.9780
a_0=7.0 mm	232.3500	242.5890	243.0600	226.5000	236.7180	238.0050	222.2040	229.5900	232.1800	214.9900	222.1200	226.2090
a_0=8.0 mm	209.6700	214.9500	223.0710	205.9300	207.0100	223.0710	200.5320	205.0500	214.3110	192.9900	198.3600	206.4510

Table 10. Ultimate rotation angle ϕ_u (rad) of joints with initial defects at different positions (left, middle, right) under constant amplitude loading systems (E, F, G, H)

Defect depths	Loading mode E (rad)			Loading mode F (rad)			Loading mode G (rad)			Loading mode H (rad)		
	Left	Middle	Right	Left	Left	Middle	Right	Left	Left	Middle	Right	Left
a_0=0.0 mm		0.0200			0.0171			0.0149			0.0123	
a_0=1.0 mm	0.0198	0.0192	0.0192	0.0161	0.0168	0.0155	0.0150	0.0149	0.0144	0.0125	0.0125	0.0118
a_0=2.0 mm	0.0155	0.0184	0.0199	0.0144	0.0175	0.0174	0.0133	0.0149	0.0150	0.0124	0.0125	0.0124
a_0=3.0 mm	0.0139	0.0143	0.0141	0.0133	0.0139	0.0138	0.0130	0.0135	0.0137	0.0125	0.0124	0.0125
a_0=4.0 mm	0.0118	0.0128	0.0141	0.0128	0.0126	0.0138	0.0122	0.0122	0.0137	0.0119	0.0119	0.0125
a_0=5.0 mm	0.0120	0.0128	0.0141	0.0116	0.0124	0.0133	0.0113	0.0128	0.0128	0.0111	0.0111	0.0123
a_0=6.0 mm	0.0108	0.0128	0.0126	0.0120	0.0124	0.0121	0.0116	0.0118	0.0120	0.0107	0.0113	0.0117
a_0=7.0 mm	0.0109	0.0116	0.0121	0.0108	0.0112	0.0116	0.0106	0.0109	0.0112	0.0103	0.0103	0.0112
a_0=8.0 mm	0.0099	0.0108	0.0116	0.0099	0.0104	0.0116	0.0095	0.0099	0.0109	0.0090	0.0095	0.0100

5. Finite element results and discussion

Table 11. Degradation characteristics of joints with initial defects at different depths under variable amplitude (B) and constant amplitude (G) loading systems

No.	Ultimate displacement δ_u (mm)	Load value corresponding to the ultimate displacement F (kN)	Bearing capacity corresponding to the amplitude displacement during unidirectional loading F_p (kN)	$\left(\frac{\Delta F}{F_p}\right)_{max}$	No.	Ultimate displacement δ_u (mm)	Load value corresponding to the ultimate displacement F (kN)	Bearing capacity corresponding to the amplitude displacement during unidirectional loading F_p (kN)	$\left(\frac{\Delta F}{F_p}\right)_{max}$
B-0	29.895	251.858	225.056	-0.119	G-0	22.500	249.692	215.790	-0.157
1-B-1	23.850	226.386	214.444	-0.056	1-G-1	22.500	234.597	215.790	-0.087
2-B-1	22.500	226.350	211.79	-0.064	2-G-1	22.500	229.514	215.790	-0.064
3-B-1	26.250	237.500	221.496	-0.072	3-G-1	22.500	221.587	215.790	-0.027
1-B-2	22.500	210.440	211.79	0.011	1-G-2	22.500	211.047	215.790	0.022
2-B-2	18.750	202.476	203.978	0.007	2-G-2	22.500	214.003	215.790	0.008
3-B-2	18.600	202.0400	203.209	0.006	3-G-2	22.500	214.781	215.790	0.005
1-B-3	17.250	184.308	194.858	0.054	1-G-3	22.500	198.673	215.790	0.079
2-B-3	17.700	185.798	197.948	0.061	2-G-3	22.500	201.506	215.790	0.066
3-B-3	18.000	186.6267	199.857	0.066	3-G-3	22.500	200.666	215.790	0.070
1-B-4	16.050	169.200	185.802	0.089	1-G-4	22.500	186.967	215.790	0.134
2-B-4	16.200	165.206	186.217	0.113	2-G-4	22.500	187.283	215.790	0.132
3-B-4	17.685	170.1333	195.85	0.131	3-G-4	22.500	188.677	215.790	0.126
1-B-5	14.700	160.518	172.553	0.070	1-G-5	22.500	175.227	215.790	0.188
2-B-5	15.000	159.896	174.238	0.082	2-G-5	22.500	172.616	215.790	0.200
3-B-5	15.000	158.4333	174.238	0.091	3-G-5	22.500	177.168	215.790	0.179
1-B-6	14.550	155.762	172.451	0.097	1-G-6	22.500	163.268	215.790	0.243
2-B-6	14.850	150.273	172.658	0.141	2-G-6	22.500	162.966	215.790	0.245
3-B-6	15.000	150.3133	174.238	0.137	3-G-6	22.500	164.487	215.790	0.238
1-B-7	12.150	128.313	142.210	0.098	1-G-7	22.500	145.365	215.790	0.326
2-B-7	13.800	126.726	146.109	0.133	2-G-7	22.500	153.065	215.790	0.291
3-B-7	11.100	120.8780	130.006	0.070	3-G-7	22.500	154.789	215.790	0.283
1-B-8	11.250	116.200	131.755	0.118	1-G-8	22.500	124.903	215.790	0.421
2-B-8	11.250	111.846	131.755	0.151	2-G-8	22.500	136.705	215.790	0.366
3-B-8	11.250	113.5133	131.755	0.138	3-G-8	22.500	142.874	215.790	0.338

5.1 Degradation characteristics

Degradation intensity is defined as the ratio of $\Delta F/F_p$. The difference value ΔF is obtained by subtracting the bearing capacity (F_p) corresponding to the monotonic loading amplitude displacement when there is no defect from the ultimate bearing capacity (F) corresponding to the actual amplitude during cyclic loading of the joint with initial defects of different depths.

Specifically, when a_0=0.0 mm, the bearing capacity corresponding to the actual amplitude during monotonic tension is F_p and when a_0=1.0 mm to 8.0 mm, the difference value between the bearing capacity (F) under the B and G loading modes and F_p is ΔF

$$Degradation\ intensity = \frac{\Delta F}{F_p} = \frac{F_p - F}{F_p}. \tag{1}$$

ΔF—The decrease in bearing capacity caused by the presence of initial defects.

F_p—The load value corresponding to the ultimate displacement of a defect-free joint under unidirectional tension.

F—The load value corresponding to the ultimate displacement of a joint with an initial defect under cyclic loading.

It can be inferred from Table 11 that as the depth of the initial defect increases, the ultimate displacement of the joint gradually decreases, and the load value corresponding to this ultimate displacement also decreases gradually.

It can be derived from the parameters corresponding to B-0, 1-B-1, 1-B-2, 1-B-3, G-0, 1-G-1, 1-G-2, and 1-G-3 that, in comparison with unidirectional tension, under the cyclic loading regime, the bearing capacity of the joint without defects (or with smaller defects) is enhanced. This phenomenon may be due to the developed plasticity of the joint, thereby resulting in a bearing capacity larger than that of unidirectional tension.

With the increase in the depth of the initial defect, the degradation characteristics of the specimen exhibit an increasing trend.

Under the condition of the same initial defect depth, within the constant amplitude or variable amplitude loading system, the position of the initial defect in the weld area of the lower flange of the beam has a negligible influence on the degradation characteristics of the joint. Hence, it can be considered that the relationship between the performance of the joint and the specific position of the initial defect is weak. Therefore, the research results presented in this article demonstrate that setting the defect at the middle position of the weld area of the lower flange of the beam can represent the situation where an initial defect exists in the weld area of the lower flange of the beam.

5.2 Damage curve

During the loading process of the joint, the damage process can be quantified based on the change in the flexural bearing capacity. In order to analyze the influence of the initial defect located at the left, middle, and right positions within the weld of the lower flange of the joint on the damage and degradation of the specimen, under the condition when a_0=0.0 mm, the ultimate bending moment value of the constant amplitude cyclic specimen is taken as the reference for each level of displacement and is regarded as the maximum bending moment of the joint in the undamaged state.

$$D = 1 - \frac{M_D}{M_u} \tag{2}$$

D—Joint damage modulus.

M_D—The maximum bending moment under the B or G loading system for each cycle, for a_0 ranging from 1.0 mm to 8.0 mm.

M_u—The ultimate bending moment under the B or G loading system for each cycle, at a_0=0.0 mm under constant amplitude cyclic loading.

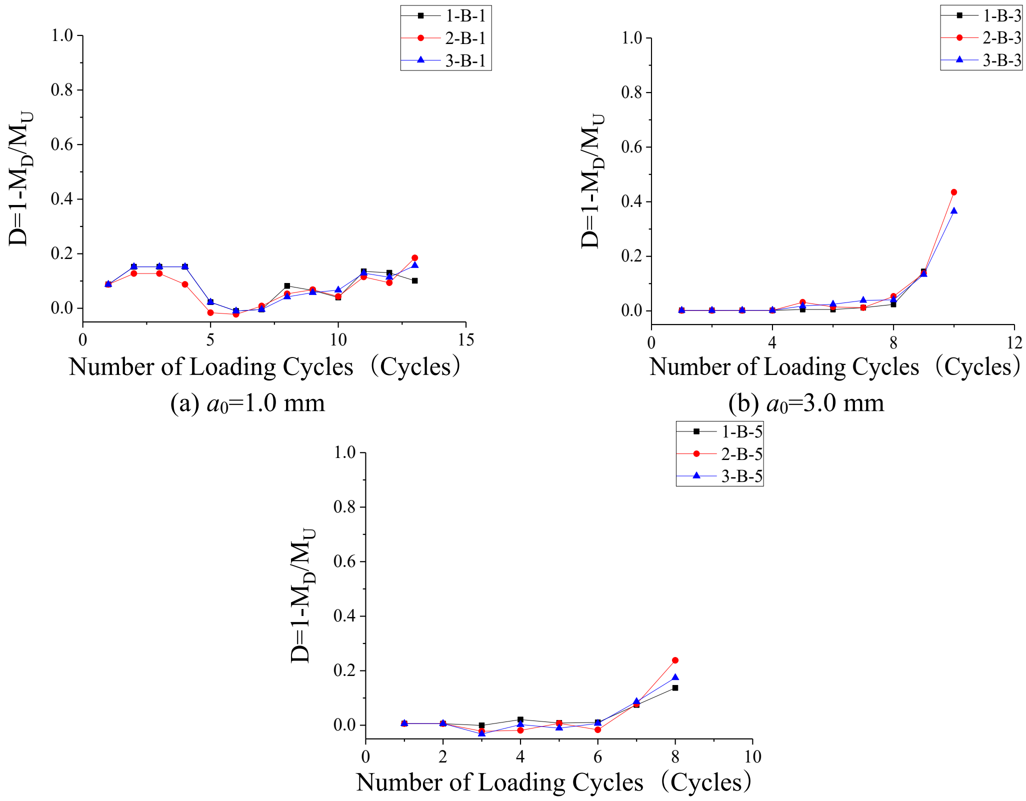

(a) a_0=1.0 mm (b) a_0=3.0 mm (c) a_0=5.0 mm

Figure 9. Damage evolution of joints with initial defects at various depths under variable amplitude loading system B

It can be observed from Figs. 9 and 10 that taking the B and G loading systems with a_0=1.0 mm, 3.0 mm, and 5.0 mm as examples, as the number of cycles increases, the amount of damage also exhibits an increasing trend. Under both the B and G loading systems, which are the variable amplitude and constant amplitude loading systems, when the initial defects of the same depth are located at the left, middle, and right positions in the weld area of the lower flange of the beam, the damage value for each cycle shows little difference. In other words, the amount of damage of the maximum bending moment value of each cycle of the specimen in the reciprocating loading process is not significantly different. Therefore, the defect positioned at the middle of the weld area of the lower flange of the beam can represent the situation where an initial defect exists in the weld area of the lower flange of the beam.

5.3 Fracture performance

The local ductility and fracture tendency of the joint can be characterized by the equivalent plastic strain index (PI) [18]. By taking the B and G loading methods, with a_0=1.0 mm, 3.0 mm, and 5.0 mm as examples, the data is presented in Table 12. Table 12 illustrates the distribution of the equivalent plastic strain index along the depth direction of the beam flange when the

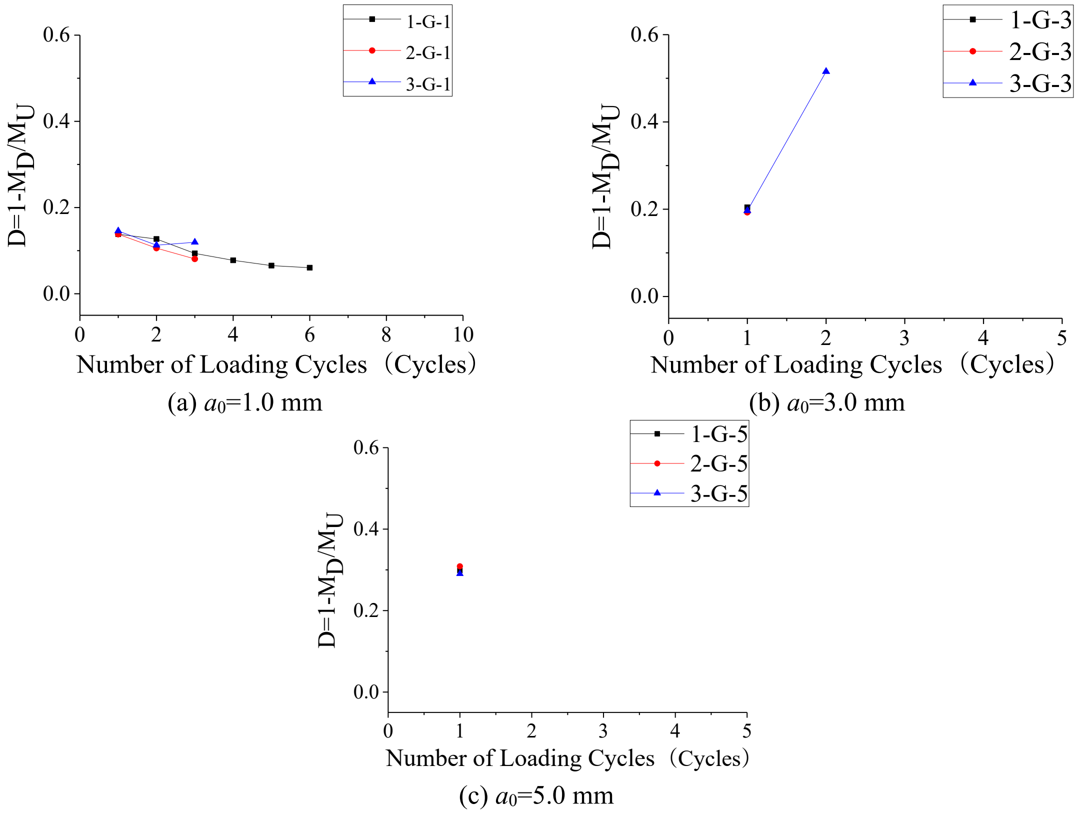

Figure 10. Damage evolution of joints with initial defects at various depths under constant amplitude loading system G

components with different initial defect depths fracture at the lower flange. Considering the components at the moment of the maximum displacement of the defect with the same depth as the research object, and selecting the path from the root of the upper and lower flanges of the beam to the points that are 0 mm, 2 mm, 4 mm, 12 mm, 27.5 mm, and 60 mm from the surface of the column to calculate the equivalent plastic strain index. It can be observed from Table 12 that under the variable amplitude and constant amplitude cyclic loading systems, as the distance from the point to the surface of the column increases, the influence of the defect position in the weld area of the lower flange of the beam on the equivalent plastic strain index of the steel gradually decreases.

It can be inferred from the failure mode, degradation characteristics, damage curve, and fracture performance that when the initial defects are located at the left, middle, and right positions in the weld of the lower flange of the beam, the differences among the four measurement indicators are not significant. This article focuses on the overall mechanical performance of the components. Therefore, the defect positioned at the middle position of the weld area of the lower flange of the beam can represent the situation where an initial defect exists in the weld area of the lower flange of the beam. It should be noted that although the maximum variation in ultimate bending moment caused by the defect location reaches 11.9%, this value represents an extreme case under specific loading and defect depth conditions. The average difference in ultimate bending moment is 3.6%, and the variation in bearing capacity induced by the defect location

Table 12. Equivalent plastic strain index (PI) at different distances from the column face for joints with initial defects under variable amplitude (B) and constant amplitude (G) loading systems

No.	0 mm		2 mm		4 mm		12 mm		27.5 mm		60 mm	
	Upper flange	Lower flange	Upper flange	Lower flange	Upper flange	Lower flange	Upper flange	Lower flange	Upper flange	Lower flange	Upper flange	Lower flange
1-B-1	2.3770	4.9544	1.8603	1.6454	4.6994	1.6326	3.4236	2.8917	9.4326	1.4241	0.7788	0.8206
2-B-1	0.2782	6.6406	0.0179	1.9578	0.0075	2.8380	1.1872	4.0622	11.1218	2.0673	1.2586	1.2596
3-B-1	0.2024	5.9261	0.0000	4.3988	0.0000	2.8334	0.0857	3.7958	10.0936	1.8874	1.0166	1.0444
1-B-3	0.0335	0.3755	0.0000	0.0092	0.0000	0.0165	0.0261	0.0464	1.9850	0.0077	0.0000	0.0000
2-B-3	0.0000	0.2150	0.0000	0.0304	0.0000	0.0000	0.0467	0.0721	2.0831	0.0164	0.0000	0.0000
3-B-3	0.0000	0.5898	0.0000	0.0133	0.0000	0.0000	0.0813	0.0816	2.1075	0.0142	0.0000	0.0000
1-B-5	25.0143	0.5141	12.3947	0.1035	6.4324	0.0000	0.6292	0.0000	2.2126	0.0000	0.0000	0.0000
2-B-5	12.5618	0.1339	33.7906	0.5108	9.3242	0.0699	0.9014	0.0000	2.5361	0.0000	0.0000	0.0000
3-B-5	3.8836	0.0349	3.0167	0.0369	1.2266	0.2873	0.8979	0.0000	2.2884	0.0000	0.0000	0.0000
1-G-1	1.4134	3.0729	0.7874	1.2903	0.9348	1.1594	2.7609	2.6689	7.9525	1.4671	0.9361	0.9793
2-G-1	0.2681	4.7611	0.0000	1.5522	0.0000	2.5659	0.3747	3.6797	8.8377	2.0401	1.1962	1.2298
3-G-1	3.0784	3.5849	1.5399	3.1133	0.0000	1.7159	2.8397	3.5021	8.0844	1.8662	0.9138	0.9603
1-G-3	1.6202	0.0017	1.2228	0.0000	2.4066	0.0695	0.8489	0.0133	0.3428	0.0079	0.0019	0.0000
2-G-3	2.5539	0.0011	1.0445	0.0000	0.0599	0.0000	1.2827	0.0250	0.3569	0.0172	0.0000	0.0000
3-G-3	3.3594	0.0410	1.6910	0.0000	0.0000	0.0000	1.8759	0.0298	0.3564	0.0192	0.0000	0.0000
1-G-5	7.5504	0.0000	9.1772	0.0000	4.9922	0.0000	0.2878	0.0000	0.2019	0.0000	0.0000	0.0000
2-G-5	0.1595	0.0000	0.1005	0.0000	0.0723	0.0000	0.0067	0.0000	0.0047	0.0000	0.0000	0.0000
3-G-5	0.1152	0.0000	0.0934	0.0000	0.0120	0.0000	0.0122	0.0000	0.0059	0.0000	0.0000	0.0000

decreases with increasing defect depth, indicating that, overall, the influence of defect location is secondary to that of defect depth. Therefore, from the perspective of engineering practice, the effect of defect location can be considered manageable provided that the influence of defect depth is properly accounted for.

6. Conclusions

This paper analyzes the influence of loading methods on joints that possess initial defects at different positions and of different depths. The research results are presented as follows:

- Regarding the influence of loading amplitude, the results indicate that loading amplitude and loading protocol have a relatively small influence on the bending moment and rotation of the joints. Based on a comparison of the three variable amplitude loading protocols (B, C, and D), the average difference in ultimate bending moment is 0.31%, with a maximum difference of 6.97%.
- Regarding the influence of initial defect depth, the skeleton of the joint without initial defects is relatively plump, and its energy dissipation capacity is superior to that of joints with defects, indicating a significant adverse effect of initial defects. Taking loading protocol B as an example, when the defect depth increases from 1.0 mm to 8.0 mm, the ultimate bending

moment decreases from 339.5800 kN·m to 174.3000 kN·m, and the ultimate rotation angle decreases from 0.0159 rad to 0.0075 rad.

• Regarding the influence of initial defect location, under loading protocols B and G, the position of the initial defect has a minor influence on the macroscopic performance of the joint. Based on a comparison of the three defect positions (left, middle, right) under loading protocol B, the maximum difference in ultimate bending moment is 11.9%, while the average difference is 3.6%. Therefore, the defect positioned at the middle of the weld area of the lower flange of the beam can represent the situation where an initial defect exists in the weld area of the lower flange of the beam.

Acknowledgements

This work was financially supported by the Start-up Fund for New Talented Researchers of Nanjing Vocational University of Industry Technology (Grant NO. YK22-06-05); the Science and Technology Project of Nanjing Construction Industry (Grant NO. Ks2261 and Grant NO. Ks2430); and the Jiangsu Provincial Double-Innovation Doctor Program (JSSCBS20220766).

Reference

1. Shi, G., Hu, F.X., Shi, Y.J. (2016). Comparison of seismic design for steel moment frames in Europe, the United States, Japan and China. Journal of Constructional Steel Research, 127(12), 41-53. https://doi.org/10.1016/j.jcsr.2016.07.009.
2. Vishnuvrdhan, S., Gandhi, P., Raghava, G., Pukazhendhi, D.M., Saravanan, M., Gupta, S.K., Bhasin, V., Vaze, K.K. (2017). Quasi-cyclic fracture studies on stainless welded straight pipes with circumferential through-wall crack in the weld. International Journal of Pressure Vessels and Piping, 149, 33-42. https://doi.org/10.1016/j.ijpvp.2016.11.005.
3. Wang, Y.Q., Zhou, H., Shi Y.Y., Chen, H. (2012). Seismic behavior analyses of welded beam-to-column connections based on fracture mechanics. Engineering Mechanics, 29(4), 104-112.
4. Wang, Y.Q., Zhou, H., Shi, Y.Y., Chen, H. (2012). Demand of beam-column connection in steel frame with thick plate column on fracture toughness. Journal of Shenyang University of Technology, 34(1), 104-110.
5. Yang, Y.T, Wang, Y., Yang, F., An, Q. (2019). Influence of weld details on fracture behavior of connections using high-strength steel. Journal of Constructional Steel Research, 153, 578-587. https://doi.org/10.1016/j.jcsr.2018.11.004.
6. Li, X., Liu, Y., Wang, Y., Yan, X., Wu, T.X., Cao, R.Z. (2022). Experimental study on seismic performance of reinforced joint of flange plate carrying crack. Journal of Guangxi University (Natural Science Edition), 47(5), 1135-1146. https://doi.org/10.13624/j.cnki.issn.1001-7445.2022.1135.
7. Huang, X.W., Tong, L.W., Zhou, F., Chen, Y.Y. (2013). Prediction of fracture behavior of beam-to-column welded joints using micromechanics damage model. Journal of Constructional Steel Research, 85, 60-72. https://doi.org/10.1016/j.jcsr.2013.02.014.
8. Ricles, J.M., Mao, C.S, Lu, L., Fisher, J.W. (2003). Ductile details for welded unreinforced moment connections subject to inelastic cyclic loading. Engineering Structures, 25(5), 667-680. https://doi.org/10.1016/S0141-0296(02)00176-1.
9. Azuma, K., Kurobane, Y., Makino, Y. (2000). Cyclic testing of beam-to-column connections with weld defects and assessment of safety of numerically modeled connections from brittle fracture. Engineering Structures, 22(12), 1596-1608. https://doi.org/10.1016/S0141-0296(99)00115-7.

10. Liu, L. (2018). Study on ductile fracture behaviors of diaphragm-Through joints considering effect of defect and access hole. M.D. Dissertation, Qingdao University of Technology, Qingdao, China.
11. Bhandari, M., Bharti, S.D., Shrimal, M.K., Datta, T.K. (2019). Seismic fragility analysis of base-isolated building frames excited by near- and far-field earthquakes. Journal of Performance of Constructed Facilities, 33(3), 04019029. https://doi.org/10.1061/(ASCE)CF.1943-5509.0001298.
12. Oyguc, E., Oyguc, R., Seker, O., Hayir, A., Shen, J., Akbas, B. (2025). Improving seismic performance of RC structures with innovative TnT BRBs: A shake table and finite element investigation. Applied Sciences, 15(7), 3844. https://doi.org/10.3390/app15073844.
13. Zuo, Y., Li, W.B. (2026). Experimental and numerical analysis of mechanical properties of steel beam-column joints with initial defects. KSCE Journal of Civil Engineering, 30(4), 100466. https://doi.org/10.1016/j.kscej.2025.100466.
14. Ministry of Housing and Urban-Rural Development of PRC (2017). GB 50017-2017: Standard for design of steel structures. China Architecture & Building Press, Beijing, China.
15. Xiong, J. (2011). Research on the damage behavior and calculation model of welded connections in steel frames under earthquake. Ph.D. Dissertation, Tsinghua University, Beijing, China.
16. Ministry of Housing and Urban-Rural Development of PRC (2015). JGJ/T 101-2015: Specification for seismic test of buildings. China Architecture & Building Press, Beijing, China.
17. Han, D., Bu, X., Wang, X.W., Jiang, C.R. (2017). Experiment on seismic performance of spatial beam to corner column connection with T-stub. Journal of Zhejiang University (Engineering Science), 51(2), 287-296. https://doi.org/10.3785/j.issn.1008-973X.2017.02.009.
18. Zhang, W.Y., Zhu, F.J. (2007). Studies on the behaviors of beam-to-column connections with beam-end flange haunch. Progress in Steel Building Structures, 6, 33-38. https://doi.org/10.3969/j.issn.1671-9379.2007.06.005.